

Ground state of doped cuprates from first-principles quantum Monte Carlo calculations

Lucas K. Wagner*

Department of Physics, University of Illinois at Urbana-Champaign, Urbana, Illinois 61801, USA

(Received 4 June 2015; revised manuscript received 15 October 2015; published 30 October 2015)

The author reports on high-fidelity simulations of charge carriers in the high- T_c cuprate materials using quantum Monte Carlo techniques applied to the first-principles Hamiltonian. With this high accuracy technique, the doped ground state is found to be a spin polaron, in which charge is localized through a strong interaction with the spin. This spin polaron has calculated properties largely similar to the phenomenology of the cuprates, and may be the object which forms the Fermi surface and charge inhomogeneity in these materials. The spin polaron has some unique features that should be visible in x-ray, EELS, and neutron experiments.

DOI: [10.1103/PhysRevB.92.161116](https://doi.org/10.1103/PhysRevB.92.161116)

PACS number(s): 71.15.-m, 74.25.-q, 74.72.Gh

I. INTRODUCTION

Understanding high temperature superconductivity in the cuprates is a long-standing and major challenge in condensed matter physics. The holes are the quasiparticles from which theories of the superconductivity are made, and in fact there have been many attempts to study doped holes using various computational and theoretical techniques. The key question is the nature of the holes upon doping from the antiferromagnetic insulating state. The combination of calculations and experiments have resulted in a substantial amount of understanding of the holes in cuprates. An important concept is spontaneous electron localization, proposed early on by authors such as Zhang and Rice [1] and Emery and Reiter [2]. These early proposals have been followed up by other authors suggesting mechanisms for electron localization [3–7]. The literature on this subject is extensive and summarized in a number of reviews [8–13].

On the experimental side, angle resolved photoemission spectroscopy (ARPES) [10,14] and quantum oscillation [15] measurements have elucidated the Fermi surface evolution as a function of doping, and generally agree on a Fermi surface that starts near $(\pi/2, \pi/2)$ in the crystallographic Brillouin zone and expands to a large pocket with doping. Optical spectroscopy [16] has found that, in addition to a Drude peak as the system becomes metallic, additional absorption in the infrared part of the spectrum appears at around 1 eV. Scanning tunneling microscopy (STM) has established that the system is inherently inhomogeneous [17–19]. Finally, neutron [20], x-ray [21], and STM techniques [17] have found that these holes can arrange in stripelike patterns.

A major theoretical challenge is that traditional electronic structure methods like density functional theory (DFT) suffer from severe errors in treatment of correlation. There have been studies using LDA+ U [22,23] and hybrid functionals [6], and using quantum chemistry techniques on cluster representations [3,7]. Recently, DFT+DMFT has been applied as well [24]. The pictures emerging from these calculations have many similarities and many differences as well. For example, while most techniques do correctly obtain holes occupying mostly the oxygen states, they disagree on whether the interaction with the copper spins is ferromagnetic or

antiferromagnetic in nature. There is a missing element in the theoretical techniques: a variational, explicitly correlated, *ab initio* calculation of the bulk material, in order to separate proposals for hole states.

In this Rapid Communication I use highly accurate quantum Monte Carlo calculations of the *ab initio* electronic structure of holes in the cuprates. This technique treats important short-range electron correlations accurately, which allows us to obtain a perspective on the effective low-energy electronic structure. It is also variational, which allows one to test different proposals for the hole state on equal footing. From these calculations, it appears that the most likely model for holes in cuprates is similar to one proposed by Emery and Reiter [2]. I will show that this hole state is consistent with the measured Fermi surface and optical spectrum, and can accommodate the formation of stripes.

The main purpose of this work is to establish the low-energy electronic structure of a hole in the cuprate material. At the level of accuracy currently feasible, quantum Monte Carlo techniques have the advantage that they are completely first principles and treat localized correlation very well; however, highly multiconfigurational wave functions are computationally out of reach given current capabilities. This work is thus concentrated on understanding the “building blocks” of the low-energy physics of the cuprates and should serve to inform effective models of their behavior. That is, if the ground state is highly multiconfigurational, then these single determinantlike states should be an important part of the correlated ground state.

II. METHOD

Fixed node diffusion Monte Carlo (FN-DMC) is a state-of-the-art method to calculate the electronic structure of materials from first principles, and has recently been found to have high accuracy for the undoped cuprates [25,26]. Starting with a trial function $|\Psi_T\rangle$, the ground state is projected out by applying the imaginary time operator $\exp(-\hat{H}\tau)$. Exact projection suffers from the sign problem, which causes the method to scale exponentially in the system size. The sign problem can be avoided by making the fixed node approximation, in which the zeros of the solution are constrained to be the same as the zeros of the trial wave function. This introduces a dependence on Ψ_T , and the energy obtained is a variational upper bound to the true ground state energy. In this work, many different Ψ_T 's

*lkwagner@illinois.edu

are considered to estimate the best approximation to the ground state of a hole in the cuprates. Details of the calculations are very similar to Ref. [26] and are recorded in the Supplemental Material [27].

The first-principles Hamiltonian was used:

$$\hat{H} = -\frac{1}{2} \sum_i \nabla_i^2 + \sum_{i<j} \frac{1}{r_{ij}} + \sum_{i\alpha} V_\alpha(r_{i\alpha}), \quad (1)$$

i, j are electron indices, α is a nuclear index, and the nuclear-nuclear interaction has been omitted for brevity. Effective core potentials from Burkatski *et al.* [28,29] were used to eliminate the core electrons and give the form for V_α . Density functional theory calculations were performed using CRYSTAL [30] to produce a starting Slater determinant, which was allowed to break spin symmetry to form localized moments. The determinant was varied by changing the starting magnetic order, which resulted in determinants with different arrangements of local moments (see Fig. 2), and by using hybrid density functional theory calculations with a varying mixing parameter. Doped systems were simulated by removing one electron from a unit cell and compensating with a uniform background charge; the minimum cell size for a given doping percentage was used. The QWalk [31] package was used to perform the quantum Monte Carlo calculations. The Slater determinant was multiplied by a two-body Jastrow factor, which was variance optimized. Diffusion Monte Carlo was then performed using the Slater-Jastrow wave function as Ψ_T . In this Rapid Communication, two cuprates are considered: CaCuO_2 , which was recently shown to be superconducting on SrTiO_3 [32], and $\text{Ca}_2\text{CuO}_2\text{Cl}_2$, which has a simple crystal structure.

In diffusion Monte Carlo, there are a number of parameters that determine the accuracy. All major parameters have been checked to the highest degree possible (Fig. 1). The time step and finite size was varied, with no changes within stochastic errors. The nodes in the input Slater determinant were varied using different hybrid density functional theories to generate the orbitals; this tuning adjusts between localized and delocalized electronic structure. The minimum energy nodal structure was taken, which was always at 25% mixing. Finally, the dependence on the interlayer was checked by considering CaCuO_2 and $\text{Ca}_2\text{CuO}_2\text{Cl}_2$ structures, with no change in the energy differences within stochastic uncertainties. As shown in Fig. 1, these parameters are converged. While the solution is not exact, in particular, long-range multiconfigurational character is not captured in this technique, these calculations are the highest accuracy *ab initio* results for a hole in the cuprates. The rest of the results in this paper will be for CaCuO_2 with $\tau = 0.02$ Hartree⁻¹, Slater determinants generated with the PBE functional at 25% exact exchange mixing [33,34], twisted boundary conditions over real twists, and T-moves [35], unless otherwise indicated.

III. RESULTS

A. Total energy

Figure 2 contains a summary of energetics for trial wave functions that differ in their magnetic ordering, for $x = 0.25$ and the $2\sqrt{2} \times 2\sqrt{2} \times 1$ supercell. The “cloverleaf” shapes are the location of the Cu atoms, with oxygen atoms between

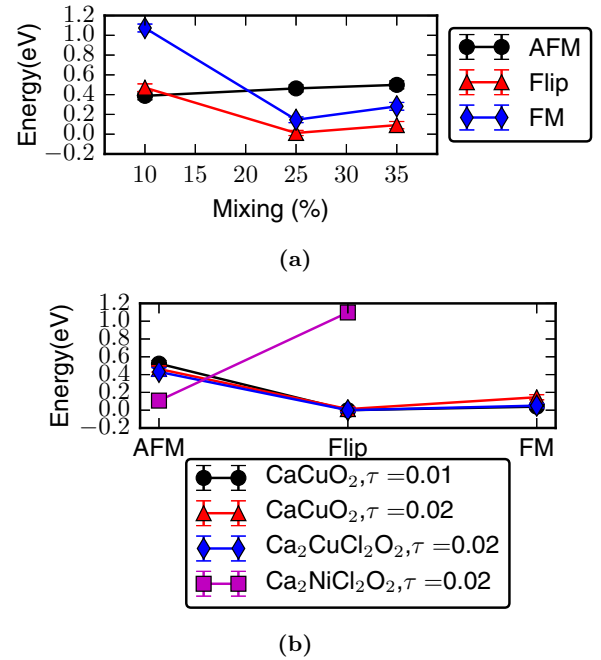


FIG. 1. (Color online) Assessing errors in the calculations for a $2 \times 2 \times 1$ supercell, with $x = 0.25$. (a) The dependence of the relative magnetic energies versus the density functional used to generate the nodes. All structures have a minimum within stochastic uncertainties at around 25% mixing. (b) At 25% mixing, the dependence on time step and on the interlayer. The physics is not qualitatively changed by these parameters. Stochastic uncertainties are approximately the size of the symbols.

them. The hole density is calculated by subtracting the doped charge density from the undoped AFM-ordered charge density. No matter the magnetic ordering, the hole density is largely situated on the oxygen atoms, in agreement with x-ray experiments. Changing the magnetic ordering affects the distribution of hole charge.

An immediately striking result in Fig. 2 is that the flipped configuration, which has a single copper atom with spin reversed from the checkerboard AFM pattern, is lowest in energy. The formation energy of this structure is the same for both the $2\sqrt{2} \times 2\sqrt{2} \times 1$ and $2 \times 2 \times 1$ supercells, and is the same for CaCuO_2 and $\text{Ca}_2\text{CuO}_2\text{Cl}_2$ (Fig. 1), so there is good reason to believe that the finite size errors are small for this quantity. The flipped spin creates a region of five copper atoms with aligned spins, and a hole is attracted mostly to the oxygen atoms between the spin-aligned atoms. The “flip” configuration is a spin polaron. The closely related compound $\text{Ca}_2\text{NiO}_2\text{Cl}_2$ does not exhibit this effect (Fig. 1), so it appears to be a special feature of the cuprates.

B. Excitation properties

The gap was computed in FN-DMC by promoting an electron in the trial Slater determinant from the highest occupied state to the lowest unoccupied state. In the case of $\text{Ca}_2\text{CuO}_2\text{Cl}_2$, the PBE0 ordering is incorrect, and the promotion was performed from the second-highest one-particle state. This was determined by trial and error; the excitation from the

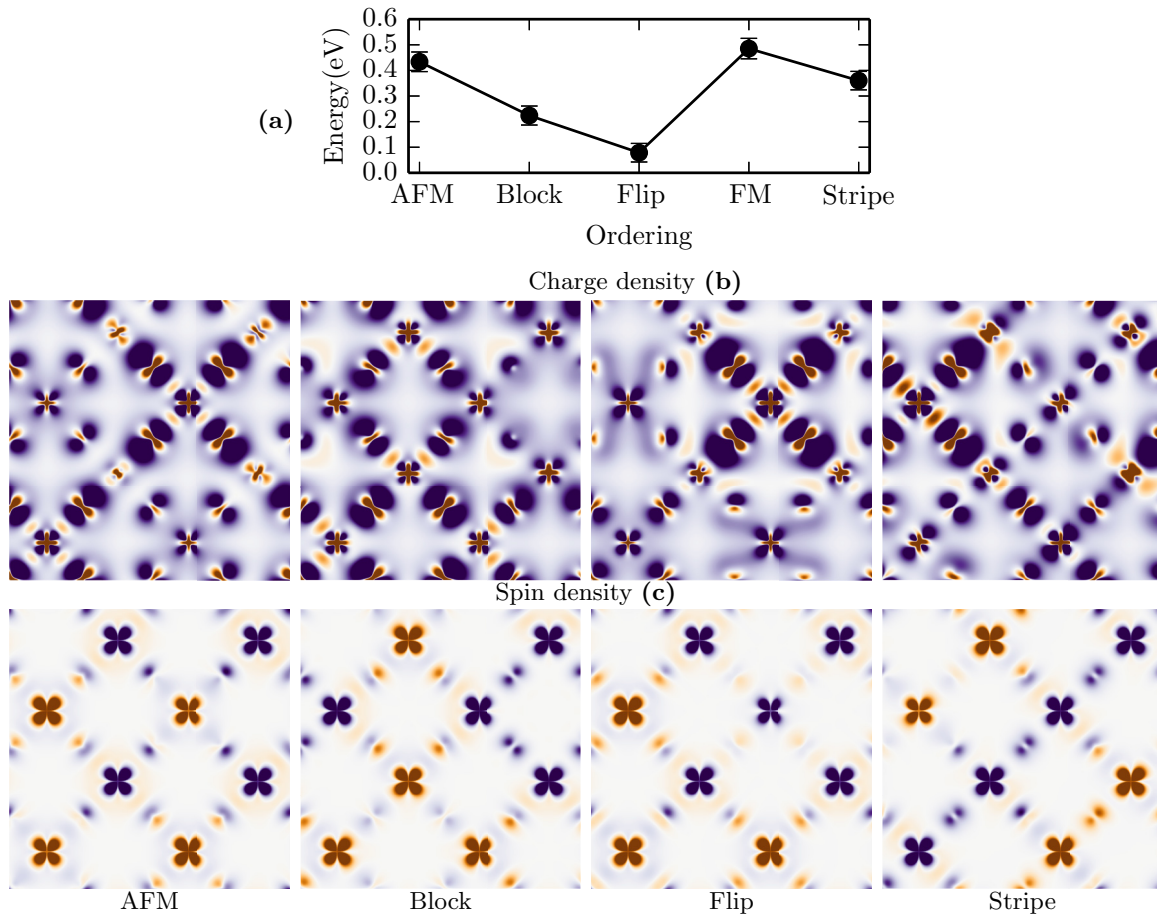


FIG. 2. (Color online) (a) FN-DMC energies of different magnetic orderings considered for a $2\sqrt{2} \times 2\sqrt{2} \times 1$ unit cell of CaCuO_2 . (b) Hole charge density obtained by subtracting the charge density of the $x = 0.125$ system from the $x = 0.00$ antiferromagnetic ordering. (c) Spin density of the corresponding orderings for $x = 0.125$. Both are calculated from the optimal single Slater determinant for that spin configuration for CaCuO_2 and projected onto the ab crystallographic plane. Correlations do not affect these pictures within statistical noise. In the density maps, blue is positive and red is negative. The density maps are normalized to the same value.

highest one-particle state was very high, around 3 eV, and involved interlayer states. For the doped configurations, both spin channels were attempted and the lower energy excitation was chosen. In Fig. 3 the gap as a function of the twisted boundary condition in the supercell are presented for the lowest energy magnetic configuration at each doping level. Because of Brillouin zone folding, the twists available are limited to the ones shown. At $x = 0.00$, the minimal gap is 2.6(1) eV, a little above the experimental gap of about 2.0 eV for the undoped cuprates. The correction for calculating the gap at the Γ point is around 0.5 eV [26], and so it is in good agreement with the experiment. Meanwhile, at $x = 0.25$, the gap clearly closes at $(\frac{1}{2}, \frac{1}{2}, 0)$, which is in agreement with ARPES.

At $x = 0.125$, it is possible that the gap closes near the Γ point $(0,0,0)$, which, accounting for band folding for the $2\sqrt{2} \times 2\sqrt{2} \times 1$ unit cell, is where the ARPES Fermi surface is located. Because of the larger supercell, the stochastic errors could not be reduced below around 0.1 eV. For CaCuO_2 , it appears that the gap is not quite closed; however, systems close to metal-insulator transitions often suffer from larger finite size effects. To check this, I also considered $\text{Ca}_2\text{CuO}_2\text{Cl}_2$ at the Γ point, which has a larger c -axis direction. It appears that the gap is either zero or near zero at the Γ point for the $\text{Ca}_2\text{CuO}_2\text{Cl}_2$

model, which increases the likelihood that the gap is actually closed at $x = 0.125$.

There is also an excitation around 1 eV that appears upon doping. This may correspond to new states seen in optical experiments at about that energy [16]. So the spin polaron configuration has excitation properties largely in agreement with those seen in experiment for the doped cuprates. Unfortunately the resolution is not high enough to comment on potential Fermi arcs.

C. Polaron-phonon coupling

While the focus of this article involves mainly the electronic degrees of freedom only, since the lowest energy state involves localized charge density, one might expect coupling to the lattice. Indeed, in the hybrid DFT calculations that also find a flipped ground state, the lattice reacts strongly to the presence of the hole, with relaxations of approximately 0.1 Å. In particular, the oxygen breathing mode is affected by the hole. This mode may be responsible for kinks in ARPES spectra [36]. These effects warrant further investigation and will likely be important for a full description of the spin polaron.

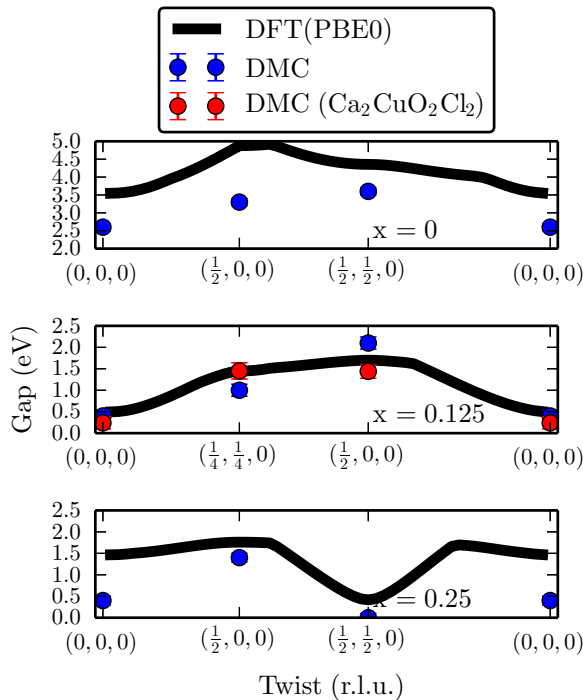


FIG. 3. (Color online) Optical gaps in FN-DMC and PBE0 calculated by promoting an electron in the Slater determinant, performed in the $2 \times 2 \times 1$ cell for $x = 0.00$ and $x = 0.25$, and in the $2\sqrt{2} \times 2\sqrt{2} \times 1$ cell for $x = 0.125$. The twisted boundary condition of the wave function in the crystallographic primitive cell is labeled on the horizontal axis.

D. Mechanism for the spin polaron

The behavior of the hole seen in the FN-DMC results warrants some explanation. Actually, the unusual behavior of magnetism in the cuprates begins even before the material is doped. In Fig. 4 the origin for both this and the spin polaron will be demonstrated for a minimal undoped two copper unit cell. As can be seen in Fig. 4(g), the oxygen has a small dipole moment of spin density that is oriented so that the spin up lobe points towards the spin up copper; that is, a ferromagnetic interaction between the oxygen lobe and the copper. This is in contrast to the normal picture, even confirmed recently in FN-DMC calculations on VO_2 [37], in which the interaction between the ligand lobe and transition metal is antiferromagneticlike. The ferromagneticlike interaction cannot be the product of a single spin-polarized orbital as can easily be checked.

In the cuprates, the spin density is primarily determined by a pair of orbitals, diagrammed in Figs. 4(a), 4(b), 4(d), and 4(e). The lower energy orbital in Figs. 4(a) and 4(b) is a low energy bonding orbital which leads to most of the spin density on the copper atoms and the normal antiferromagnetic relationship of the oxygen lobes with the copper spins, as seen in Fig. 4(c). The higher energy orbital in Figs. 4(d) and 4(e) is partially antibonding and leads to a reversed spin density [compare Figs. 4(c) and 4(f)]. The sum of these two spin densities, Fig. 4(g), now has a ferromagnetic relationship between the copper spin and the oxygen lobes.

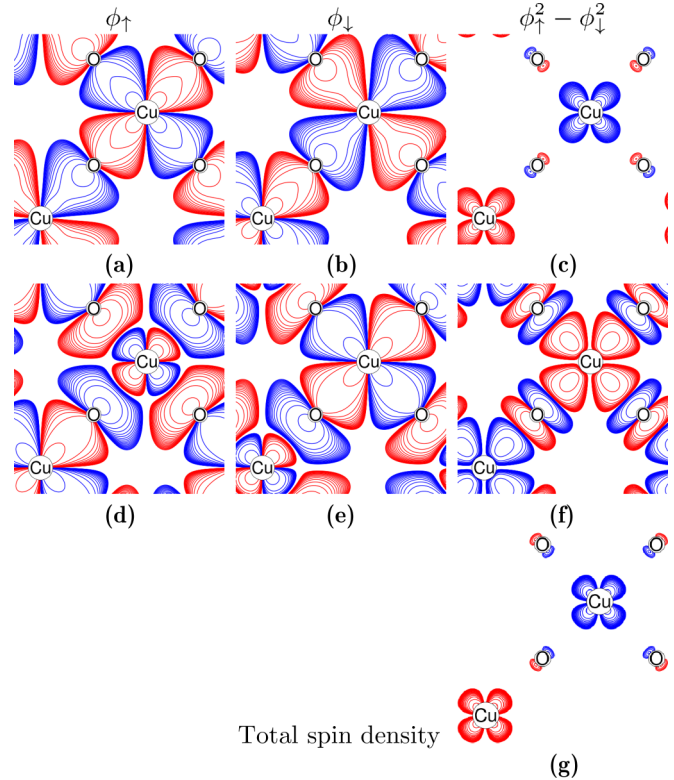


FIG. 4. (Color online) Orbitals contributing to the spin density of a two formula unit cell of CaCuO_2 . (a)–(c) Lower energy orbital that contributes to most of the spin density on the copper atoms. (d)–(f) Higher energy orbital that contributes to most of the spin density on the oxygen atoms. (g) Sum of the two spin densities, which accounts for most of the total spin density. Blue is positive, red is negative.

On doping, the partially antibonding orbital is depopulated. Since this orbital affects the coupling between adjacent copper spins, the interaction changes from antiferromagnetic to ferromagnetic. In the FN-DMC calculations, we see that the spin up/spin down covariance on the copper atom around which the hole is centered decreases from -0.05 to -0.02 , which is due to a decrease in the double occupancy of that copper atom. In addition, the orbital is partially antibonding, which costs kinetic energy. The spin polaron, therefore, is stabilized by a balance between the kinetic energy and the interaction energy between electrons, which necessitates a correlated approach like FN-DMC.

E. Charge and spin stripes

Patterson [6] noted that in hybrid DFT (B3LYP) calculations, it was possible to form charge and spin density waves using spin polarons. In Fig. 5 a similar structure is presented, along with the Fourier transform of the charge and spin. Since the QMC calculations agree with DFT(PBE0) on the ground state density, it is likely good enough to analyze the properties of such a stripe system. The stripe structure in Fig. 5 is in several ways quite close to that seen in neutron, x-ray, and STM experiments. It matches the Bragg peak in the charge density at $(0.25, 0)$, as well as a d -wave intracell density, as seen in STM [17].

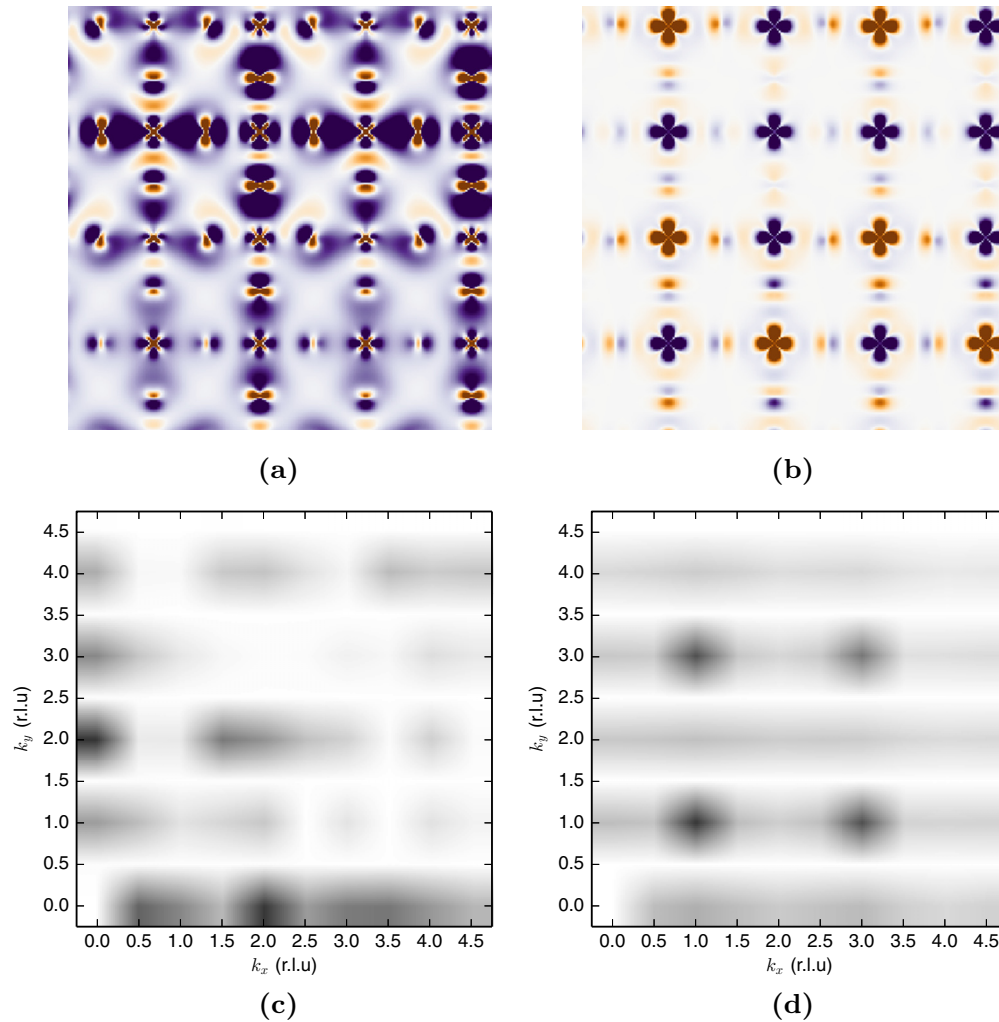


FIG. 5. (Color online) Charge (a) and spin (b) density in PBE0 for two holes in a $4 \times 4 \times 1$ supercell. The corresponding Fourier transforms for charge (c) and spin (d) have a Bragg peak at $(0,0.125)$ because of the periodicity in addition to the plotted values. The k values are in units of the reciprocal lattice of the primitive tetragonal crystallographic cell.

If these stripes of spin polarons are the objects responsible for the stripes in the cuprates, then there should be a small peak in neutron diffraction at $(1,0)$ and $(0,1)$ due to the FM-like coupling between the copper atoms [Fig. 5(d)], in addition to AFM-like $(1,1)$ peaks. This peak is a necessary prediction of this physics; if it is not present, then these objects cannot be responsible for the stripes. On the other hand, the Fourier transform of the charge density should have small peaks at $(0.5,0.25)$ from the periodicity of the charge density. These small peaks are necessary for this structure to exist, and could be used to falsify these spin polarons as the origin of the stripes.

IV. CONCLUSION

In summary, the microscopic physics of doped cuprates has been studied using state of the art quantum Monte Carlo techniques. The properties are very close to that seen in experiment, with the Fermi surface near that of the experiment, and optical excitations in agreement. The metal-insulator transition of the cuprates likely occurs between $x = 0.00$ and $x = 0.125$, which means that this transition has been captured accurately within a first-principles method. In a few years, it

will likely be possible to use these techniques to study the metal-insulator transition in detail. Much of the phenomenology of the cuprates is consistent with the picture emerging from the FN-DMC results. This is a particularly exciting result, since the FN-DMC methodology employed here does not use any effective parametrization of the interactions, it is a predictive methodology that could be helpful in the search for materials with similar physics.

The picture emerging from the FN-DMC calculations is that of a spin polaron. The particular polaron found in this work was to my knowledge first proposed by Emery and Reiter [2] early on, and has been considered by a number of authors since then [6]. The uniqueness of this study is that (1) it is truly first principles and explicitly correlated, with no adjustable parameters, (2) it was shown that the spin polaron can lead to a similar Fermi surface structure as seen in experiment, and (3) there are new predictions which allow the proposal to be evaluated experimentally. This spin polaron can be further studied using quantum Monte Carlo techniques, and it will be fruitful to study the properties of this quasiparticle; for example, the interaction between two spin polarons. It is possible that similar but related structures appear at larger

supercell sizes, but it seems clear that the basic physics will remain the same. This spin polaron is not stable in the closely related material $\text{Ca}_2\text{NiO}_2\text{Cl}_2$, and thus may be one reason for the uniqueness of the cuprates.

ACKNOWLEDGMENTS

I would like to thank the many people who contributed comments to this paper, in particular Hitesh Changlani,

David Ceperley, J. C. Seamus Davis, Awadhesh Narayan, Mike Norman, and Huihuo Zheng. This material is based upon work supported by the U.S. Department of Energy, Office of Science, Office of Advanced Scientific Computing Research, Scientific Discovery through Advanced Computing (SciDAC) program under Award Number FG02-12ER46875. Computational resources were provided by the DOE INCITE SuperMatSim and PhotoSuper programs.

-
- [1] F. C. Zhang and T. M. Rice, *Phys. Rev. B* **37**, 3759 (1988).
 [2] V. J. Emery and G. Reiter, *Phys. Rev. B* **38**, 4547 (1988).
 [3] R. L. Martin, *Phys. Rev. B* **53**, 15501 (1996).
 [4] N. Mott, *Adv. Phys.* **39**, 55 (1990).
 [5] B. Lau, M. Berciu, and G. A. Sawatzky, *Phys. Rev. Lett.* **106**, 036401 (2011).
 [6] C. H. Patterson, *Phys. Rev. B* **77**, 094523 (2008).
 [7] L. Hozoi, S. Nishimoto, and C. de Graaf, *Phys. Rev. B* **75**, 174505 (2007).
 [8] M. Hashimoto, I. M. Vishik, R.-H. He, T. P. Devereaux, and Z.-X. Shen, *Nat. Phys.* **10**, 483 (2014).
 [9] E. Dagotto, *Rev. Mod. Phys.* **66**, 763 (1994).
 [10] A. Damascelli, Z. Hussain, and Z.-X. Shen, *Rev. Mod. Phys.* **75**, 473 (2003).
 [11] V. Z. Kresin and S. A. Wolf, *Rev. Mod. Phys.* **81**, 481 (2009).
 [12] D. J. Scalapino, *Rev. Mod. Phys.* **84**, 1383 (2012).
 [13] C. C. Tsuei and J. R. Kirtley, *Rev. Mod. Phys.* **72**, 969 (2000).
 [14] E. Razzoli, Y. Sassa, G. Drachuck, M. Mnsson, A. Keren, M. Shay, M. H. Berntsen, O. Tjernberg, M. Radovic, J. Chang *et al.*, *New J. Phys.* **12**, 125003 (2010).
 [15] N. Doiron-Leyraud, C. Proust, D. LeBoeuf, J. Levallois, J.-B. Bonnemaïson, R. Liang, D. A. Bonn, W. N. Hardy, and L. Taillefer, *Nature (London)* **447**, 565 (2007).
 [16] F. Cilento, S. D. Conte, G. Coslovich, F. Banfi, G. Ferrini, H. Eisaki, M. Greven, A. Damascelli, D. v. d. Marel, F. Parmigiani *et al.*, *J. Phys.: Conf. Ser.* **449**, 012003 (2013).
 [17] K. Fujita, C. K. Kim, I. Lee, J. Lee, M. H. Hamidian, I. A. Firmo, S. Mukhopadhyay, H. Eisaki, S. Uchida, M. J. Lawler *et al.*, *Science* **344**, 612 (2014).
 [18] H. Mashima, N. Fukuo, Y. Matsumoto, G. Kinoda, T. Kondo, H. Ikuta, T. Hitosugi, and T. Hasegawa, *Phys. Rev. B* **73**, 060502 (2006).
 [19] W. D. Wise, M. C. Boyer, K. Chatterjee, T. Kondo, T. Takeuchi, H. Ikuta, Y. Wang, and E. W. Hudson, *Nat. Phys.* **4**, 696 (2008).
 [20] J. M. Tranquada, B. J. Sternlieb, J. D. Axe, Y. Nakamura, and S. Uchida, *Nature (London)* **375**, 561 (1995).
 [21] P. Abbamonte, A. Ruydi, S. Smadici, G. D. Gu, G. A. Sawatzky, and D. L. Feng, *Nat. Phys.* **1**, 155 (2005).
 [22] P. Rivero, I. de P. R. Moreira, R. Grau-Crespo, S. N. Datta, and F. Illas, *Phys. Rev. B* **88**, 085108 (2013).
 [23] S. Pesant and M. Cote, *Phys. Rev. B* **84**, 085104 (2011).
 [24] C. Weber, K. Haule, and G. Kotliar, *Nat. Phys.* **6**, 574 (2010).
 [25] K. Foyevtsova, J. T. Krogel, J. Kim, P. R. C. Kent, E. Dagotto, and F. A. Reboredo, *Phys. Rev. X* **4**, 031003 (2014).
 [26] L. K. Wagner and P. Abbamonte, *Phys. Rev. B* **90**, 125129 (2014).
 [27] See Supplemental Material at <http://link.aps.org/supplemental/10.1103/PhysRevB.92.161116> for energetic data and detailed computational settings.
 [28] M. Burkatzki, C. Filippi, and M. Dolg, *J. Chem. Phys.* **126**, 234105 (2007).
 [29] M. Burkatzki, C. Filippi, and M. Dolg, *J. Chem. Phys.* **129**, 164115 (2008).
 [30] R. Dovesi, R. Orlando, B. Civalleri, C. Roetti, V. R. Saunders, and C. M. Zicovich-Wilson, *Z. Kristallogr.* **220**, 571 (2005).
 [31] L. K. Wagner, M. Bajdich, and L. Mitás, *J. Comput. Phys.* **228**, 3390 (2009).
 [32] D. Di Castro, C. Cantoni, F. Ridolfi, C. Aruta, A. Tebano, N. Yang, and G. Balestrino, *Phys. Rev. Lett.* **115**, 147001 (2015).
 [33] J. P. Perdew, K. Burke, and M. Ernzerhof, *Phys. Rev. Lett.* **77**, 3865 (1996).
 [34] C. Adamo and V. Barone, *J. Chem. Phys.* **110**, 6158 (1999).
 [35] M. Casula, *Phys. Rev. B* **74**, 161102 (2006).
 [36] D. R. Garcia and A. Lanzara, *Adv. Condens. Matter Phys.* **2010**, 1 (2010).
 [37] H. Zheng and L. K. Wagner, *Phys. Rev. Lett.* **114**, 176401 (2015).